



Molecular Doping of Near-Infrared Organic Photodetectors for Photoplethysmogram Sensors

Journal:	<i>Journal of Materials Chemistry C</i>
Manuscript ID	TC-ART-11-2020-005549.R1
Article Type:	Paper
Date Submitted by the Author:	03-Jan-2021
Complete List of Authors:	<p>Wang, Binghao; University of Tokyo Graduate School of Engineering Department of Electrical Engineering and Information Systems Scaccabarozzi, Alberto; KAUST, KSC Wang, Haoyang; University of Tokyo Graduate School of Engineering Department of Electrical Engineering and Information Systems Koizumi, Mari; University of Tokyo Graduate School of Engineering Department of Electrical Engineering and Information Systems Nugraha, Mohamad; King Abdullah University of Science and Technology, Physical Sciences and Engineering Lin, Yuanbao; King Abdullah University of Science and Technology Physical Sciences and Engineering Division, Materials Science and Engineering Firdaus, Yuliar; King Abdullah University of Science and Technology, Wang, Yan; The University of Tokyo, Lee, Sunghoon; University of Tokyo Graduate School of Engineering Department of Electrical Engineering and Information Systems Yokota, Tomoyuki; The University of Tokyo, Anthopoulos, Thomas; King Abdullah University of Science and Technology Physical Sciences and Engineering Division, Materials Science and Engineering Someya, Takao; University of Tokyo Graduate School of Engineering Department of Electrical Engineering and Information Systems, ; RIKEN, Thin-Film Device Laboratory & Center for Emergent Matter Science</p>

COMMUNICATION

Molecular Doping of Near-Infrared Organic Photodetectors for Photoplethysmogram Sensors

Received 00th January 20xx,
Accepted 00th January 20xx

Binghao Wang,^a Alberto D. Scaccabarozzi,^b Haoyang Wang,^a Koizumi Mari,^a Mohamad Insan Nugraha,^b Yuanbao Lin,^b Yuliar Firdaus,^b Yan Wang,^a Sunghoon Lee,^a Tomoyuki Yokota,^{*,a} Thomas D. Anthopoulos^{*,b} and Takao Someya^{*,a}

DOI: 10.1039/x0xx00000x

Doping is a common strategy in the field of semiconductor technology but its employment in organic photodetectors (OPDs) has been limited due to the typical uncontrollable increase of the dark currents. This study introduces three different molecular dopants, including *p*-type tris(pentafluorophenyl)borane, *n*-type benzyl viologen, and (4-(1,3-dimethyl-2,3-dihydro-1H-benzimidazol-2-yl)-phenyl)dimethylamine, for near-infrared poly(3-hexylthiophene-2,5-diyl): [6,6]-phenyl C₆₁ butyric acid methyl ester bulk-heterojunction OPDs. Results show that OPDs with optimal 0.02 wt% dopants exhibit low dark current (3.18×10⁻⁸ A cm⁻²), high detectivity (5.56×10¹² Jones) and good environmental stability for ~2 months. These doped OPDs are further used for pulse wave monitoring and exhibit stable waveform for slow and fast heartbeat rates.

Introduction

Organic semiconductors (OSCs) are normally used in their intrinsic form (i.e. not intentionally doped), in strong contrast to their inorganic counterpart that exploits doping as the basis of the devices functionality.¹ Nevertheless, doping of OSCs played a major role in the development of high efficiency organic electronic devices. Indeed, dopants have been used to fabricate highly conducting layers, capable of lowering the ohmic losses, upon adjusting the Fermi levels and hence, ultimately improving charge injection/collection at the electrodes.²⁻⁶ Conducting layers rely on the introduction of relatively high amounts of doping molecules, on the order of percent.^{7, 8, 9} However, the addition of dopants directly in the active layer of electronic devices at ultra-low concentrations has been recently gaining an increasing interest, leading to a substantial improvement of

performance in organic thin film transistors (OTFTs)^{6, 10, 11} and solar cells.^{3, 7, 12, 13} The beneficial effect of doping is ascribed to a number of phenomena including improved charge transport¹⁴ and microstructure¹⁵, traps passivation in OTFTs,⁶ while improving exciton splitting,^{16, 17} suppressing carrier recombination¹⁸ and improved morphology¹⁹ in solar cells.

To improve the organic device performance, the doping strategy has been extensively used also for organic light-emitting diodes,^{20, 21} organic thermoelectrics,²²⁻²⁴ and organic-based batteries.^{25, 26} Recently, very few studies on doping of organic photodetectors (OPDs) have been reported.^{27, 28} Tian et al. reported near-infrared photodetectors based on iodine-doped poly(3-hexylthiophene-2,5-diyl): [6,6]-phenyl C₆₁ butyric acid methyl ester (P3HT:PCBM) blend.²⁷ With iodine doping, the resulting OPDs exhibited resistor-like behaviour in the dark and had high specific responsivity ($R \sim 80 \text{ A W}^{-1}$), specific detectivity ($D^* \sim 1.6 \times 10^{12}$ Jones), and external quantum efficiency ($EQE \sim 120\%$) under near-infrared irradiation (NIR) illumination with a wavelength of 850 nm.

However, maintaining low dark current and long-term stability after doping is challenging. First, the doping process generally produces free charges, which typically increase the conductivity of semiconductor layers. Second, most dopants are not environmentally stable and the system's free charges could degrade the device performance significantly.

Here we show how the addition of low concentrations of molecular dopants to the bulk heterojunction OPDs led to improved current under illumination without detrimentally increasing the dark current and simultaneously improving the long-term environmental stability. Three different molecular dopants, including *p*-type tris(pentafluorophenyl)borane (BCF), *n*-type benzyl viologen (BV), and (4-(1,3-dimethyl-2,3-dihydro-1H-benzimidazol-2-yl)-phenyl)dimethylamine (N-DMBI), have been introduced and compared. Results show that OPDs with optimal dopant (0.02 wt%) exhibit low dark current, high detectivity and good storage stability. After storing in ambient for more than two months, the BV-doped near-infrared (NIR) OPDs without encapsulation still work well for the pulse wave

^a Department of Electrical and Electronic Engineering and Information Systems, The University of Tokyo, 7-3-1 Hongo, Bunkyo-ku, Tokyo, 113-8656 Japan. E-mail: yokota@ntech.t.u-tokyo.ac.jp, someya@ee.t.u-tokyo.ac.jp

^b King Abdullah University of Science and Technology (KAUST), KAUST Solar Center (KSC), Thuwal, 23955 Saudi Arabia. E-mail: thomas.anthopoulos@kaust.edu.sa
Electronic Supplementary Information (ESI) available: [details of any supplementary information available should be included here]. See DOI: 10.1039/x0xx00000x

monitoring, which exhibits stable waveform and can distinguish slow and fast heartbeat rates.

Results and discussion

Fig. 1a shows the chemical structures of the polymer donor Poly[[2,5-bis(2-hexyldecyl)-2,3,5,6-tetrahydro-3,6-dioxopyrrolo[3,4-c]pyrrole-1,4-diyl]-alt-[3',3''-dimethyl-2,2':5',2''-terthiophene]-5,5''-diyl] (PMDPP3T), the acceptor PCBM, and the dopants of BV, BCF and N-DMBI. Dopant containing formulations were prepared by adding the desired amount of dopant solution into the PMDPP3T:PCBM blends with a weight ratio of 1:3. The concentrations of dopants were calculated as a weight percentage of the solid weight mass of the donor and acceptor materials (see the Experimental Section in SI). As shown in Fig. 1b, indium tin oxide (ITO), deposited on glass, was used as transparent electrode in an inverted OPD architecture. The surface of ITO was coated with a ZnO layer to adjust the work function of the electrode with respect to the lowest unoccupied molecular orbital (LUMO) of the PCBM. After

spin-coating the active layer, the device fabrication was finalized by thermally evaporating MoO_x as the hole transport layer and Ag as top electrode. Fig. 1c shows the energy levels of the various materials and electron/hole transport under illumination. Previous reports from our group and others' labs indicated that the highest occupied molecular orbital (HOMO) levels of BV, BCF and N-DMBI are -3.3 eV, -7.2 eV and -4.4 eV, respectively.^{7, 22, 29, 30} These three dopants have very different doping mechanism. Specifically, the HOMO of the neutral BV is higher than the LUMO (-4.0 eV) of the PCBM acceptor molecules, providing a favourable energetic landscape for electron transfer from BV to PCBM and resulting n-type doping.^{7, 31, 32} Regarding the BCF, its energy levels would suggest that it should not participate as a p-dopant due to its high LUMO (-3.2 eV).³³ The doping mechanism of this molecular additive is related to its Lewis acid character, which can withdraw electron from a π -system by forming highly polarized complexes where H₂O is known to play a role.^{34, 35} Regarding N-DMBI, its highly efficient doping mechanism is based on thermally activated hydride transfer reactions, as widely reported in previous works.^{22, 24}

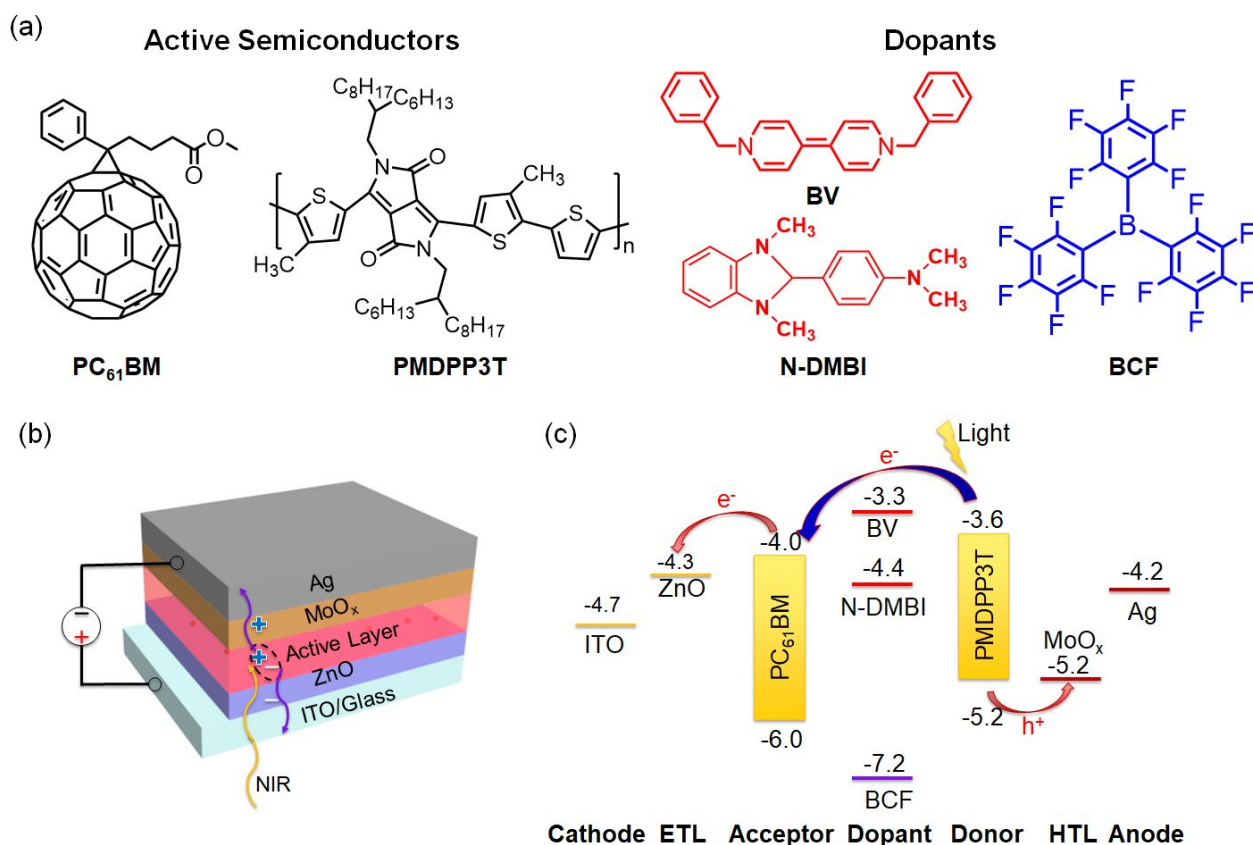


Fig. 1. (a) Chemical structures of organic semiconductors and dopants used in OPD devices. (b) A schematic device structure of OPD devices. (c) Energy band for different functional materials and charge transport process of an OPD device during illumination.

The current density–voltage (J - V) characteristics of undoped and doped PMDPP3T:PCMB OPDs in the dark and under irradiation (2.64 mW cm⁻²) at a wavelength of 850 nm are shown in Fig. 2a-2c and their dark current densities (J_d) are summarized in Fig. 2d and Table 1. The J_d of undoped OPD is 3.07×10^{-8} A cm⁻² at -2 V, while under illumination, the current

density (J_{ph}) at -2 V significantly increases by five orders of magnitude, reaching 1.41 mA cm⁻². Moreover, the undoped OPD exhibits J_{ph} of 0.15 mA cm⁻² at 0 V under illumination and has an open-circuit voltage (V_{oc}) of ~0.6 V. These results are comparable with previous reports.^{36, 37} For comparison, the OPDs doped with 0.02 wt% BV exhibit an increased J_{ph} of 1.48

mA cm⁻² and 0.25 mA cm⁻² at -2 V and 0 V, respectively. However, when the amount of dopant is increased to 0.5 wt%, the J_{ph} decreases to 1.24 mA cm⁻² and 0.05 mA cm⁻² at -2 V and 0 V, respectively. Interestingly, the J_d at -2 V only slightly increases to 3.18×10⁻⁸ A cm⁻² when 0.02 wt% BV is added to the system, while a more substantial increase to 8.6×10⁻⁸ A cm⁻² is observed for the higher concentration 0.5 wt% BV. Regarding the BCF doping, the J_{ph} at -2 V of OPDs with 0.02 wt% and 0.5 wt% BCF are 1.49 mA cm⁻² and 0.65 mA cm⁻², respectively. The J_d at -2 V increases with higher BCF concentrations and reaches 7.2×10⁻⁷ A cm⁻² for 0.5 wt% BCF. In terms of N-DMBI doping, the J_{ph} at -2 V is 1.39 mA cm⁻² and 0.75 mA cm⁻² for OPDs with 0.02 wt% and 0.5 wt% dopants, respectively. However, due to the strong doping ability, the J_d at -2 V increases significantly and reaches to 1.4 ×10⁻⁵ A cm⁻² for OPDs with 0.5 wt% N-DMBI,

which is 2-3 orders of magnitudes higher than that of undoped devices and BV-doped OPDs. Nevertheless, an ultra-low concentration of all dopants (0.02 wt%) does not lead to a detrimental increase of dark current, while the J_{ph} is increased. The photo responsivity (R_{ph}) and detectivity (D^*) are two other important parameters for OPDs, calculated from equation 1 and 2, respectively.

$$R_{ph} = (J_{ph} - J_d) / L_{ph} \quad (1)$$

$$D^* = \frac{R_{ph}}{(2qJ_d)^{1/2}} \quad (2)$$

Where L_{ph} is the light intensity and q is the absolute value of electron charge.^{38, 39} Since dark currents in this work originate from a low electron injection barrier, the shot noise would indeed be a dominant factor and the use of Equation 2 will not obviously affect the calculation of D^* .^{40, 41}

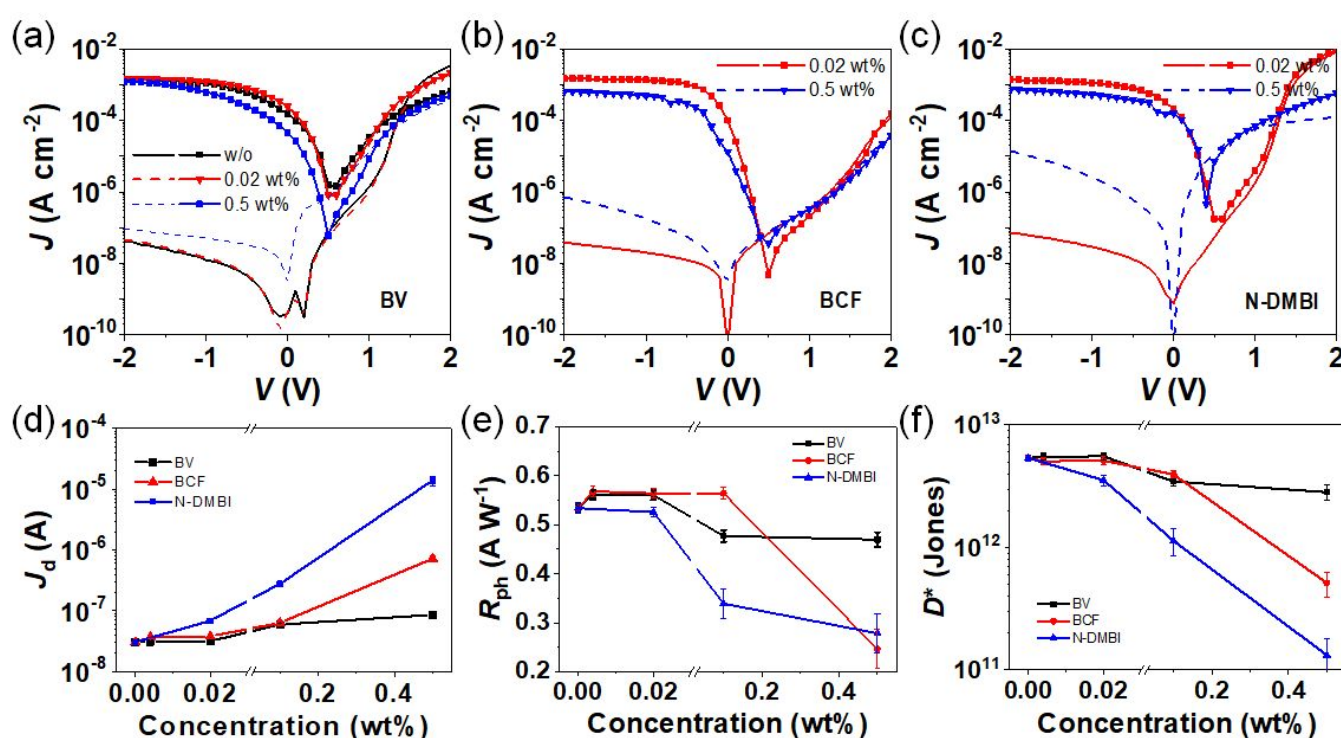


Fig 2. J - V curves of PMDPP3T:PCBM OPDs in the dark (dashed lines) and under NIR illumination with a wavelength of 850 nm (solid lines) doped with (a) BV, (b) BCF and (c) N-DMBI. Dependence of (d) dark current density (J_d), (e) Responsivity (R_{ph}) and (f) specific detectivity (D^*) on dopant types and concentrations when driven at -2 V.

Table 1. Performance metrics of undoped and doped PMDPP3T:PCBM OPDs.^a

	J_d (10 ⁻⁸ A cm ⁻²)	J_{ph} (10 ⁻³ A cm ⁻²)	J_{ph}/J_d	R_{ph} (A W ⁻¹)	D^* (10 ¹² Jones)
Undoped	3.07±0.21	1.41±0.02	4.59±0.02×10 ⁴	0.53±0.01	5.39±0.22
0.02 wt% BV	3.18±0.23	1.48±0.02	4.65±0.02×10 ⁴	0.56±0.01	5.56±0.25
0.5 wt% BV	8.59±0.62	1.24±0.02	1.44±0.03×10 ⁴	0.47±0.12	2.83±0.32
0.02 wt% BCF	3.81±0.27	1.49±0.02	3.91±0.02×10 ⁴	0.56±0.01	5.11±0.28
0.5 wt% BCF	72.12±8.13	0.65±0.03	9.01±0.05×10 ²	0.25±0.04	0.51±0.12
0.02 wt% N-DMBI	6.89±0.48	1.39±0.02	2.02±0.03×10 ⁴	0.52±0.01	3.54±0.20
0.5 wt% N-DMBI	1390.17±253.57	0.75±0.03	53.95±2.65	0.28±0.04	0.13±0.05

^aData is collected from 12 devices.

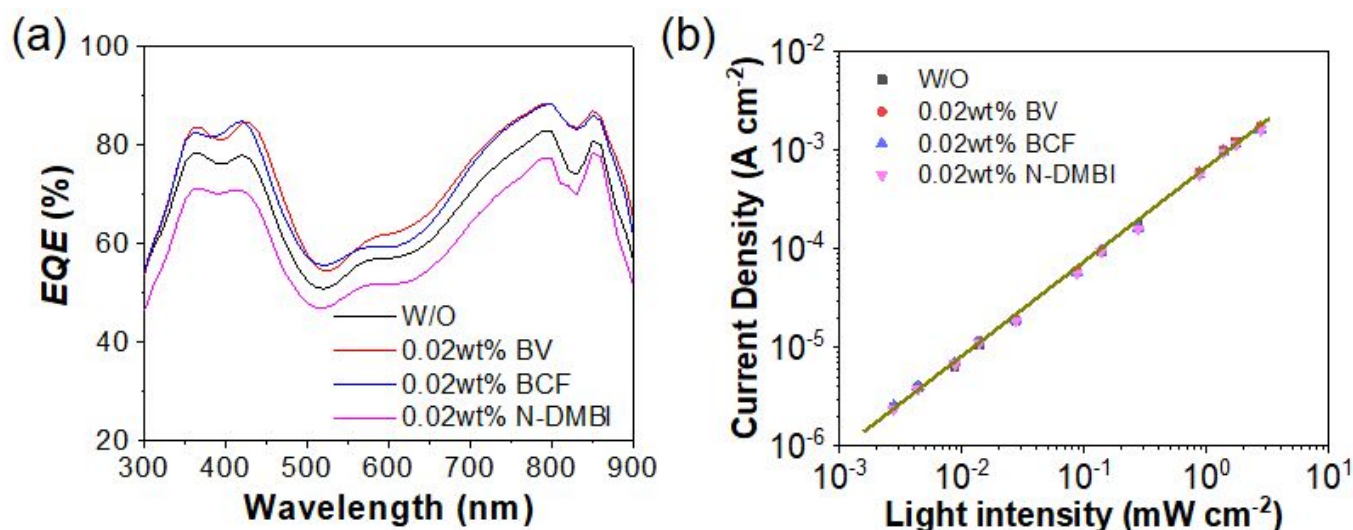


Fig 3. (a) EQE of undoped and 0.02 wt% doped PMDPP3T:PCBM OPDs under -2 V bias. (b) The relationship between current density at -2 V and light intensity for doped and 0.02 wt% undoped PMDPP3T:PCBM OPDs.

Fig. 2e and 2f summarize the R_{ph} and D^* measured at -2 V for undoped and doped OPDs with different dopants and concentrations. The undoped OPDs have an R_{ph} of 0.53 A W^{-1} and D^* of 5.39×10^{12} Jones, comparable to those of silicon photodiodes ($\sim 0.6 \text{ A W}^{-1}$ and 10^{12} - 10^{13} Jones).³⁷ OPDs doped with BV at ultra-low concentration (0.02 wt%) exhibit an increased R_{ph} of 0.56 A W^{-1} and D^* of 5.56×10^{12} Jones, while higher concentrations lead to decreased values reaching 0.47 A W^{-1} and 2.83×10^{12} Jones for 0.5 wt%. Similar trend is observed for BCF devices. A low concentration of BCF, 0.02 wt%, leads to an increase J_{ph} of 1.49 mA cm^{-2} , while the dark current is only slightly affected, $J_d = 3.81 \text{ mA cm}^{-2}$, hence leading to R_{ph} of 0.56 A W^{-1} and D^* of 5.11×10^{12} Jones. OPDs doped with BCF and N-DMBI show a substantial decrease of performance for doping concentrations above 0.1 wt%. Indeed, both the R_{ph} and D^* decrease significantly reaching $0.25/0.28 \text{ A W}^{-1}$ and $5.1/1.3 \times 10^{11}$ Jones for 0.5 wt% BCF and 0.5 wt% N-DMBI, respectively. As discussed above, the three dopants have different doping mechanisms, but all these doping mechanisms can be highly efficient and lead to an increase of electrical conductivity by several orders of magnitudes at optimized dopant concentrations, indeed they have been widely reported in organic thermoelectric applications. On the other hand, high conductivity has a detrimental effect on OPD performance upon increasing dark current, as it is clear in our 0.5 wt% devices. However, ultra-low concentrations of dopants lead to improved responsivity and detectivity due to the increased currents under illumination, while dark currents remain only slightly affected. Thus, there is an optimization window for OPDs, leading to improved performance.

Another parameter that describes the photoelectric conversion capability of an OPD is the external quantum efficiency (EQE), that is defined as the ratio between the number of photogenerated electrons and the incoming photons. Fig. 3a and 3b show the EQE, i.e., the spectral response of undoped and doped OPDs under illuminated conditions and -2 V bias voltage. The undoped OPDs exhibit a high EQE over

50% in the whole spectral range (300-900 nm) and reach 80.9% at a wavelength of 850 nm. For OPDs doped with 0.02 wt% BV and BCF, the EQE increases over the whole wavelength range and reaches as high as 87.0% and 86.1% at a wavelength of 850 nm, respectively. Concerning N-DMBI doping, an obvious decrease in EQE is observed. The EQE at a wavelength of 850 nm is 78.5% for OPDs with 0.02 wt% N-DMBI. We also measure the J_{ph} of undoped and 0.02 wt% doped OPDs with various light intensities. As shown in Fig. 3c, all the OPDs exhibit good linearity with $R > 99\%$ even when light intensity decreases to only $2.75 \times 10^{-3} \text{ mW cm}^{-2}$. The J_{ph} s for all the four OPDs illuminated at $2.75 \times 10^{-3} \text{ mW cm}^{-2}$ are still in the level of $10^{-6} \text{ A cm}^{-2}$, two orders of magnitudes higher than those in the dark. Moreover, from the J_{ph} -intensity curve, we can extract the linear dynamic range (LDR). LDR is a useful parameter that provides information about the contrast of the photodetector and is calculated as the ratio of photocurrent at maximum light intensity to photocurrent at minimum light intensity in decibels.⁴² The extracted LDRs exhibit ~ 60 dB for all test devices (limited by measurement range), which is comparable to that of an InGaAs photodetector.^{43,44}

Another important parameter for photodetectors is the dynamic characteristics' response speed. We hence measured their temporal response to 850 nm NIR (Fig. 4) and analyzed the response and recovery time. Given a fixed incident light intensity, the response time and recovery time are mainly dependent on the charge carrier transport in the device.⁴⁵⁻⁴³ Note that the turn-on and turn-off measurements were conducted separately and manually. Thus, the absolute values of current density is slightly different, however, the response and recovery time of these OPD devices will not be affected. The reference OPDs and those fabricated with BV doping (0.02 wt% and 0.5 wt%) exhibit the fast response time of $\sim 16 \mu\text{s}$. The photocurrents exhibit a transient overshoot which has been already reported in other systems and it is typically associated with charge trapping, i.e. a part of photo-generated electrons contribute to occupy trap states in the system and a build-up of

charge carrier occurs.^{46,47} For OPDs with 0.02 wt% BCF and 0.02 wt% N-DMBI doping, the photocurrents reach steady state without experiencing any overshoot, which is probably due to a stronger doping ability of BCF and DMBI, when compared with that of BV and hence to a more efficient trap filling. As a consequence, photo-generated charge carriers do not contribute to the occupancy of trap states and the transient overshoot is not observed.⁴⁶ However, the response times increase significantly when more BCF and N-DMBI are added, as they disrupt the electronic properties of the system. The response times reach 126 μs and 291 μs for OPDs with 0.5 wt%

BCF and 0.5 wt% N-DMBI, respectively. Regarding the recovery time, the OPDs with and without BV dopant have a similar recovery time of 25–26 μs , it decreases to 18–19 μs when 0.02 wt% BCF and N-DMBI are added, possibly due to traps passivation. However, the recovery time increases significantly, reaching 200 μs and 700 μs when 0.5 wt% BCF and N-DMBI are added, respectively. At such a high concentration, charge carrier mobility is significantly affected and the balance between p- and n-type charges is broken.⁷ Thus the charge transport becomes much less efficient.

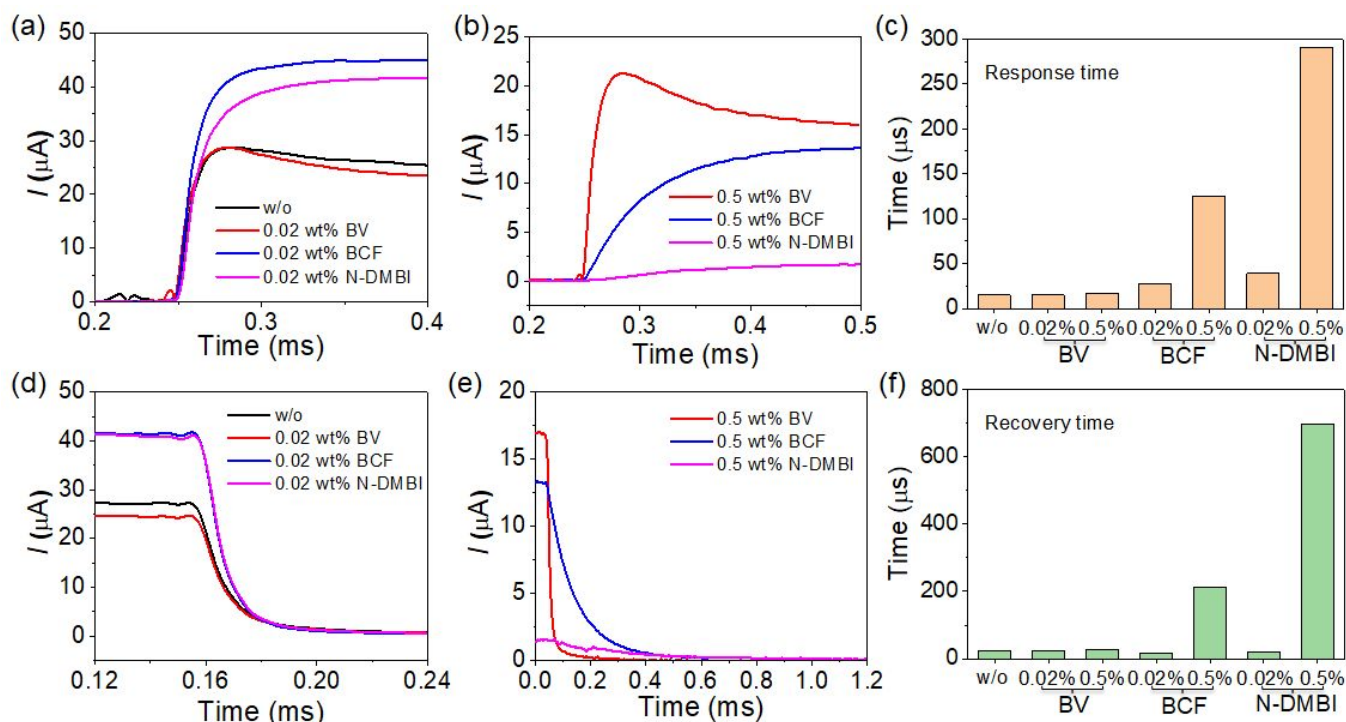


Fig 4. (a) Dynamic response for pristine OPDs and those with 0.02 wt% dopants, (b) Dynamic response for OPDs with 0.5 wt% dopants. (c) Summarized Response time for OPDs with and without dopants. (d) Dynamic recovery for pristine OPDs and those with 0.02 wt% dopants, (e) Dynamic recovery for OPDs with 0.5 wt% dopants. (f) Summarized recovery time for OPDs with and without dopants.

Device stability is a critical issue typically observed in a wide range of organic electronic devices. To test the stability of our OPDs, the un-encapsulated devices have been measured for multiple times during 63 days' storage both in N_2 and air (Fig. 5a and Fig. S1). When devices are stored in a N_2 filled glovebox, the D^* s initially decrease, regardless the composition, possibly due to the semiconductor layer's reorganization with the desorption of O_2 and H_2O .⁴⁸ Then all the D^* s increase significantly after 13 days of storage in N_2 , with two devices outperforming the fresh devices. The increased D^* s are mainly due to the decreased dark current (Fig. S2). We then exposed the devices to ambient conditions and measured the evolution of the PD characteristics over time. Overall, we can observe a sharp decrease in D^* after one day for all the doped and undoped OPDs. After that, undoped devices and those comprising 0.02 wt% BV and BCF show a gradual drop of D^* s over time. Interestingly, devices comprising 0.02 wt% N-DMBI shows a recovering of the device parameters after 20 days of air exposure. These results show that n-doped OPD devices appear more air stable than undoped and p-type doped OPD devices, possibly due to the air-stabile doping ability of

the n-type dopants. After 63 days' storage, the OPDs with 0.02 wt% BV exhibit 65% of original D^* value, while undoped OPDs are only 50% of original D^* value.

Finally, we demonstrate a transmissive pulse oximeter using a NIR LED, and the OPD doped with 0.02 wt% BV (Figure 5b). The NIR LED had an intensity of 30 mW cm^{-2} , the J_{ph} of the OPD, biased at -2 V, is monitored to measure the absorption of NIR light by the blood. Fig. 5c shows the J_{ph} of fresh OPDs and 63 days-stored OPDs in a 30 s measured range. Two different statuses (at rest and after running) of the healthy tester are monitored. From the enlarged plots (Fig. 5d and 5e), we know that the devices work well even after long-term storage in ambient. The generated Photoplethysmogram (PPG) signals exhibit good repeatability for both statuses. The J_{ph} of OPD exhibits strong fluctuation ($\Delta J_{\text{ph}}/J_{\text{ph}}$ is 8.6%) when the person is tested after running, higher than that (2.4%) of OPDs tested at rest. From the frequency plot processed by fast Fourier transform (Fig. 5f), the former exhibits a faster pulse rate (88 beats/min) than that (58 beats/min) tested at rest.

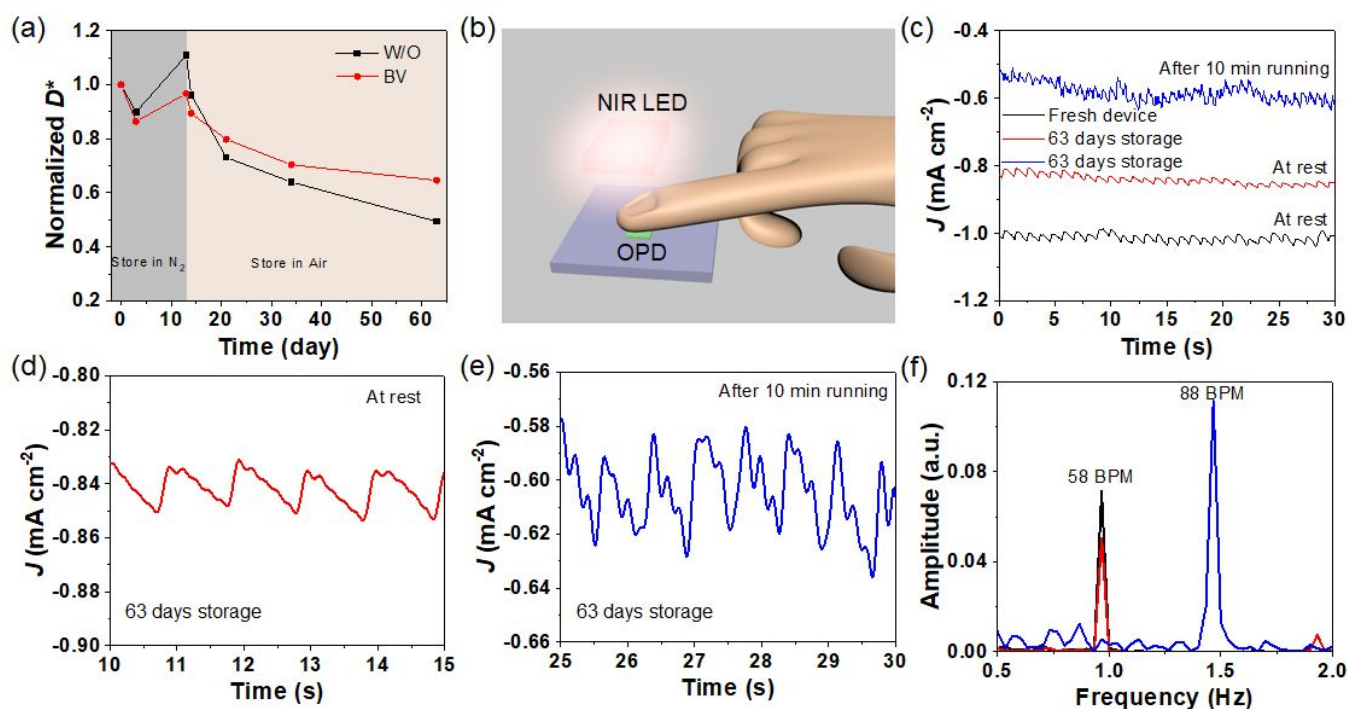


Fig 5. (a) The D^* stability of OPDs without and with 0.02 wt% dopants in N_2 and air atmosphere. (b) Schematic image of pulse wave test based on NIR LED and OPD system. (c) the current density and (d-e) enlarged plots for current density at rest and after 10 min running. (f) Pulse frequency processed by fast Fourier transform.

Conclusions

In summary, we have demonstrated the effects of various molecular dopants on the OPD performance. OPDs fabricated with ultra-low amounts of BV, and BCF dopants exhibit low dark current, high responsivity, and high detectivity, outperforming non-doped devices. However, the performance degrades significantly when more than 0.1 wt% dopants are added. The addition of the N-DBMI dopant detrimentally increases the dark current; thus, the performance of N-DBMI-doped OPDs degrade gradually as increasing the dopant amount. The addition of molecular dopants also leads to an improvement in device stability. The unencapsulated 0.02 wt% BV-doped OPDs exhibit better environmental stability than undoped ones and perform well for pulse wave monitoring after 63 days' storage. We expect that the fabrication of doped-OPDs on flexible substrates could be integrated into emerging wearable electronics for future Internet of Things applications.

Conflicts of interest

There are no conflicts to declare.

Acknowledgements

This work was financially supported by collaborative research program (OSR#4196) between the University of Tokyo (UTokyo) and King Abdullah University of Science and Technology (KAUST) and Japan Science and Technology Agency (JST) ACCEL

(grant no. JPMJMI17F1) We thank to Dr. Sixing Xiong (Riken) for the helpful discussion.

References

1. Y. Xiong, J. J. Zeng, B. Chen, J. W. Y. Lam, Z. J. Zhao, S. M. Chen and B. Z. Tang, *Chinese Chem Lett*, 2019, **30**, 592-596.
2. X. Guo and A. Facchetti, *Nat Mater*, 2020, **19**, 922-928.
3. I. Salzmann and G. Heimel, *J Electron Spectrosc Relat Phemon*, 2015, **204**, 208-222.
4. K. P. Madhuri, N. S. John, S. Angappane, P. K. Santra and F. Bertram, *J. Phys. Chem. C*, 2018, **122**, 28075-28084.
5. D. Khim, K.-J. Baeg, M. Caironi, C. Liu, Y. Xu, D.-Y. Kim and Y.-Y. Noh, *Adv. Funct. Mater.*, 2014, **24**, 6252-6261.
6. A. F. Paterson, Y.-H. Lin, A. D. Mottram, Z. Fei, M. R. Niazi, A. R. Kirmani, A. Amassian, O. Solomeshch, N. Tessler, M. Heeney and T. D. Anthopoulos, *Adv Electron Mater*, 2018, **4**, 1700464.
7. Y. Lin, Y. Firdaus, M. I. Nugraha, F. Liu, S. Karuthedath, A. H. Emwas, W. Zhang, A. Seitkhan, M. Neophytou, H. Faber, E. Yengel, I. McCulloch, L. Tsetseris, F. Laquai and T. D. Anthopoulos, *Adv. Sci.*, 2020, **7**, 1903419.
8. D. Kiefer, R. Kroon, A. I. Hofmann, H. Sun, X. Liu, A. Giovannitti, D. Stegerer, A. Cano, J. Hynnen, L. Yu, Y. Zhang, D. Nai, T. F. Harrelson, M. Sommer, A. J. Moule, M. Kemerink, S. R. Marder, I. McCulloch, M. Fahlman, S. Fabiano and C. Muller, *Nat Mater*, 2019, **18**, 149-155.
9. I. E. Jacobs and A. J. Moule, *Adv. Mater.*, 2017, **29**, 1703063.
10. Y. Han, Z. Fei, Y.-H. Lin, J. Martin, F. Tuna, T. D. Anthopoulos and M. Heeney, *npj Flexible Electronics*, 2018, **2**, 11.
11. X. Zhang, B. Wang, L. Huang, W. Huang, Z. Wang, W. Zhu, Y. Chen, Y. Mao, A. Facchetti and T. J. Marks, *Sci. Adv.*, 2020, **6**, eaaz1042.

12. F. A. Larrain, C. Fuentes-Hernandez, W. F. Chou, V. A. Rodriguez-Toro, T.-Y. Huang, M. F. Toney and B. Kippelen, *Energy Environ. Sci.*, 2018, **11**, 2216-2224.
13. M. Y. Chan, S. L. Lai, M. K. Fung, C. S. Lee and S. T. Lee, *Appl. Phys. Lett.*, 2007, **90**, 023504.
14. A. D. Scaccabarozzi, F. Scuratti, A. J. Barker, A. Basu, A. F. Paterson, Z. Fei, O. Solomeshch, A. Petrozza, N. Tessler, M. Heeney, T. D. Anthopoulos and M. Caironi, *Adv Electron Mater*, 2020, **6**, 2000539.
15. A. Basu, M. R. Niazi, A. D. Scaccabarozzi, H. Faber, Z. Fei, D. H. Anjum, A. F. Paterson, O. Boltalina, M. Heeney and T. D. Anthopoulos, *J. Mater. Chem. C*, 2020, **8**, 15368-15376.
16. Y. Zhang, H. Zhou, J. Seifert, L. Ying, A. Mikhailovsky, A. J. Heeger, G. C. Bazan and T. Q. Nguyen, *Adv. Mater.*, 2013, **25**, 7038-7044.
17. A. Loiudice, A. Rizzo, M. Biasiucci and G. Gigli, *J Phys Chem Lett*, 2012, **3**, 1908-1915.
18. D. Zhang, Q. Li, J. Zhang, J. Wang, X. Zhang, R. Wang, J. Zhou, Z. Wei, C. Zhang, H. Zhou and Y. Zhang, *ACS Appl. Mater. Interfaces*, 2020, **12**, 667-677.
19. H. Yan, J. Chen, K. Zhou, Y. Tang, X. Meng, X. Xu and W. Ma, *Adv. Energy Mater.*, 2018, **8**, 1703672.
20. S. J. Kwon, T. H. Han, Y. H. Kim, T. Ahmed, H. K. Seo, H. Kim, D. J. Kim, W. Xu, B. H. Hong, J. X. Zhu and T. W. Lee, *ACS Appl. Mater. Interfaces*, 2018, **10**, 4874-4881.
21. K. T. Wong, R. T. Chen, F. C. Fang, C. C. Wu and Y. T. Lin, *Org Lett*, 2005, **7**, 5925-5925.
22. Y. Zeng, W. Zheng, Y. Guo, G. Han and Y. Yi, *J Mater Chem A*, 2020, **8**, 8323-8328.
23. K. Shi, F. Zhang, C. A. Di, T. W. Yan, Y. Zou, X. Zhou, D. Zhu, J. Y. Wang and J. Pei, *J. Am. Chem. Soc.*, 2015, **137**, 6979-6982.
24. H. I. Un, S. A. Gregory, S. K. Mohapatra, M. Xiong, E. Longhi, Y. Lu, S. Rigin, S. Jhulki, C. Y. Yang, T. V. Timofeeva, J. Y. Wang, S. K. Yee, S. Barlow, S. R. Marder and J. Pei, *Adv. Energy Mater.*, 2019, **9**, 1900817.
25. J. Luder, F. Legrain, Y. Q. Chen and S. Manzhos, *MRS Communications*, 2017, **7**, 523-540.
26. A. Wild, M. Strumpf, B. Haupler, M. D. Hager and U. S. Schubert, *Adv. Energy Mater.*, 2017, **7**, 1601415.
27. P. Tian, L. Tang, J. Xiang, Z. Sun, R. Ji, S. K. Lai, S. Ping Lau, J. Kong, J. Zhao, C. Yang and Y. Li, *RSC Adv.*, 2016, **6**, 45166-45171.
28. R. O. Ocaya, A. Al-Ghamdi, K. Mensah-Darkwa, R. K. Gupta, W. Farooq and F. Yakuphanoglu, *Synth. Met.*, 2016, **213**, 65-72.
29. H. Kim and T. N. Ng, *Adv Electron Mater*, 2018, **4**, 1700631.
30. M. I. Nugraha, S. Kumagai, S. Watanabe, M. Sytnyk, W. Heiss, M. A. Loi and J. Takeya, *ACS Appl. Mater. Interfaces*, 2017, **9**, 18039-18045.
31. G. Huseynova, N. K. Shrestha, Y. Xu, E.-Y. Shin, W.-T. Park, D. Ji and Y.-Y. Noh, *Org. Electron.*, 2018, **62**, 572-580.
32. D.-H. Lee, M. Kang, D.-H. Lim, Y. Kim, J. Lee, D.-Y. Kim and K.-J. Baeg, *J. Mater. Chem. C*, 2018, **6**, 5497-5505.
33. E. J. Lawrence, V. S. Oganessian, G. G. Wildgoose and A. E. Ashley, *Dalton Trans*, 2013, **42**, 782-789.
34. C. R. Bridges and T. Baumgartner, *Journal of Physical Organic Chemistry*, 2020, **33**, e4077.
35. B. Yurash, D. X. Cao, V. V. Brus, D. Leifert, M. Wang, A. Dixon, M. Seifrid, A. E. Mansour, D. Lungwitz, T. Liu, P. J. Santiago, K. R. Graham, N. Koch, G. C. Bazan and T. Q. Nguyen, *Nat Mater*, 2019, **18**, 1327-1334.
36. S. Xiong, J. Tong, L. Mao, Z. Li, F. Qin, F. Jiang, W. Meng, T. Liu, W. Li and Y. Zhou, *J. Mater. Chem. C*, 2016, **4**, 1414-1419.
37. T. Yokota, T. Nakamura, H. Kato, M. Mochizuki, M. Tada, M. Uchida, S. Lee, M. Koizumi, W. Yukita, A. Takimoto and T. Someya, *Nature Electronics*, 2020, **3**, 113-121.
38. L. Ye, H. Li, Z. Chen and J. Xu, *ACS Photonics*, 2016, **3**, 692-699.
39. G. Simone, M. J. Dyson, S. C. J. Meskers, R. A. J. Janssen and G. H. Gelinck, *Adv. Funct. Mater.*, 2019, **30**, 1904205.
40. Y. Fang, A. Armin, P. Meredith and J. Huang, *Nature Photonics*, 2018, **13**, 1-4.
41. I. K. Kim, J. H. Jo, J. Lee and Y. J. Choi, *Org. Electron.*, 2018, **57**, 89-92.
42. C. X. Bao, Z. L. Chen, Y. J. Fang, H. T. Wei, Y. H. Deng, X. Xiao, L. L. Li and J. S. Huang, *Adv. Mater.*, 2017, **29**, 1703209.
43. S. B. Lim, C. H. Ji, I. S. Oh and S. Y. Oh, *J. Mater. Chem. C*, 2016, **4**, 4920-4926.
44. Z. Lan, Y. Lei, W. K. E. Chan, S. Chen, D. Luo and F. Zhu, *Sci Adv*, 2020, **6**, eaaw8065.
45. X. Liu, Y. Lin, Y. Liao, J. Wu and Y. Zheng, *J. Mater. Chem. C*, 2018, **6**, 3499-3513.
46. Y. Wang, L. Zhu, Y. Hu, Z. Deng, Z. Lou, Y. Hou and F. Teng, *Opt Express*, 2017, **25**, 7719-7729.
47. C. R. McNeill, I. Hwang and N. C. Greenham, *J. Appl. Phys.*, 2009, **106**, 024507.
48. M. Kielar, O. Dhez, G. Pecastaings, A. Curutchet and L. Hirsch, *Sci Rep*, 2016, **6**, 39201.